Anomalous, non-Gaussian, viscoelastic, and age-dependent dynamics of histonelike nucleoid-structuring proteins in live Escherichia coli

Asmaa A. Sadoon and Yong Wang

Phys. Rev. E **98**, 042411 — Published 19 October 2018

DOI: 10.1103/PhysRevE.98.042411

Anomalous, non-Gaussian, viscoelastic and age-dependent dynamics of histone-like H-NS proteins in live *Escherichia coli*

Asmaa A. Sadoon and Yong Wang*
Department of Physics, Microelectronics and Photonics Program, Cell and Molecular Biology Program, University of Arkansas, Fayetteville, AR 72701
(Dated: July 29, 2018)

We report our measurements of the dynamics of H-NS proteins, which interact with both proteins and DNA simultaneously, in live *E. coli* bacteria. The dynamics turn out to differ significantly from other molecules reported previously. A new power-law distribution was observed for the diffusion coefficients of individual H-NS proteins. In addition, we observed a new distribution of displacements, which does not follow the Gaussian, Cauchy, or Laplace distributions, but the Pearson Type VII distribution. Furthermore, we experimentally measured, for the first time, the time/frequency dependence of the complex modulus of the bacterial cytoplasm, which deviates from the viscoelasticity of homogeneous protein solutions and shows a glass-liquid transition. Lastly, we observed that the dynamics of H-NS protein is cell-length/cell-age dependent. The findings are expected to fundamentally change the current views on bacterial cytoplasm and diffusional dynamics of molecules in bacteria.

I. INTRODUCTION

Dynamic diffusion of molecules inside cytoplasm is vital for bacteria, as transport and mixing of cytoplasmic molecules and resources primarily rely on diffusion, due to the small size of bacteria and lack of active transport mechanisms [1]. Although the diffusion of particles and molecules in various solutions and environments has been extensively studied both theoretically and experimentally, quantitative knowledge on the dynamic diffusion of biological molecules inside live bacteria remains relatively limited [2]. Single-particle tracking (SPT) has become a standard method for studying the dynamics of molecules in live bacteria and cells [1–5]; furthermore, the recent development of super-resolution fluorescence microscopy [6–10] in combination with SPT has allowed tracking individual molecules at high densities (commonly termed as sptPALM [11]), opening a new avenue. This technique has been applied to several biological molecules, such as RNA polymerases, ribosomes, antimicrobial peptides, and transcription factors [12–15], providing new quantitative clues on the relevant fundamental processes in live systems as well as the interactions between the molecules and the intracellular environment.

Despite the exciting progresses, a gap exists towards a full understanding of the dynamics of molecules in live systems. The molecules examined in the previous studies include standalone proteins or DNA/RNA molecules, and proteins that interact with DNA or RNA [1, 3–5, 12–15]; however, there are many molecules in the cells interacting with both proteins and DNA (and other cellular components) simultaneously. One example is the ParMRC system for plasmid segregation [16]. Another example is the histone-like nucleoid-structuring protein (H-NS) [17]. H-NS, one of the nucleoid associated proteins in bacteria, regulates (mostly negatively) 5% of the bacterial genome [18]. It consists of a DNA binding domain, an oligomerization domain, and a linker connecting the two domains [17]. Therefore, H-NS not only binds to (and unbinds from) DNA, but also interacts with themselves to form polymers as well as DNA-bridging structures (Fig. 1A) [17]. It has been shown that both oligomerization and DNA binding are crucial for the biological activities of H-NS proteins [17].

In this work, we present our results on the dynamics of H-NS proteins in live *Escherichia coli* (*E. coli*) bacteria, which shows unique behaviors compared to other molecules reported previously. We observed a new power-law distribution of the diffusion coefficients of individual H-NS proteins and a new distribution of displacements that does not follow the Gaussian, Cauchy, or Laplace distributions, but the Pearson Type VII distribution. More importantly, for the first time, we experimentally measured the time/frequency dependence of the complex modulus of the bacterial cytoplasm, which deviates from the viscoelasticity of homogeneous protein solutions and shows a glass-liquid transition. Finally, we found that the dynamics of H-NS protein is dependent on cell-age. The findings are expected to fundamentally change the current views on bacterial cytoplasm and diffusional dynamics of molecules in bacteria.

II. METHODS AND MATERIALS

A. Bacterial strain, growth, and sample preparation

A K12-derived *E. coli* strain (a gift from [19]) was used in this study. This strain expresses H-NS proteins fused to mEos3.2 fluorescent proteins [19, 20]. The bacterial strain was grown at 37°C overnight in defined M9 minimal medium, supplemented with 1% glucose, 0.1% casamino acids, 0.01% thiamine and appropriate antibi-

* yongwang@uark.edu

otics (kanamycin + chloramphenicol) [21]. On the second day, the overnight culture was diluted by 50 to 100 times into fresh medium so that the OD600 was 0.05. The fresh cultures were again grown at 37°C. When the OD600 reaches ∼0.3, 10 μL of the bacteria were transferred to a 5mm × 5mm agarose pad (3% in the growth medium). The sample was left at room temperature for 20–30 minutes, allowing the bacterial cells absorbed into the agarose pad. The agarose pad was then flipped and attached to a clean coverslip (cleaned with sonication in 1M NaOH, 100% ethanol, and ultra-pure water sequentially). A chamber was then constructed by sandwiching a rubber o-ring between the coverslip and a microscope slide. The chamber was sealed using epoxy glue and incubated at room temperature for ∼1 hours in dark before imaging, to prevent water evaporation and shrinkage of the agarose pad during data acquisition.

B. Super-resolution fluorescence imaging and single-particle tracking (sptPALM)

The super-resolution fluorescence microscope was home-built on an Olympus IX-73 inverted microscope with an Olympus TIRF 100X N.A.=1.49 oil immersion objective. The microscope and data acquisition were controlled by Micro-Manager [22]. A 405 nm laser and a 532 nm laser from a multilaser system (iChrome MLE, TOPTICA Photonics, NY) were used to "activate" and excite mEos3.2-HNS fusion proteins in bacteria. Emissions from the fluorescent proteins were collected by the objective and imaged on an EMCCD camera (Andor, MA) with an exposure time of 30 ms. The effective pixel size of acquired images was 160 nm; and the actual interval between frames was 45 ms.

The resulting movies (20,000 frames) were analyzed with RapidStorm [23], generating x/y positions, x/y widths, intensity, and background for each detected fluorescent spot. Spots with localization precisions >40 nm were rejected. The positions $\mathbf{r}(t)$ from the same molecule in adjacent frames were linked by standard algorithms with a memory of one frame and a maximum step size of 0.48 μm [11, 12, 24], from which the trajectories of individual molecules $\mathbf{r}(t)$ were obtained.

III. RESULTS AND DISCUSSIONS

A. Anomalous and heterogeneous diffusion of H-NS proteins

SptPALM was used to track the motion of H-NS proteins in live *E. coli*, as illustrated in Fig. 1B and described in "Methods and Materials". Reconstructing super-resolved images from the positions $\mathbf{r}$ of the activated, fluorescent proteins showed that H-NS proteins formed small clusters (Fig. 1C), consistent with previous results [19, 25]. The positions of H-NS proteins were linked as described and examples of H-NS proteins' trajectories in individual bacteria in an area of 8×8 μm^2 were shown in Fig. 1D. Large heterogeneity was observed (Fig. 1E): some H-NS proteins were confined in small regions (red curves) while some showed large displacements (green curves).

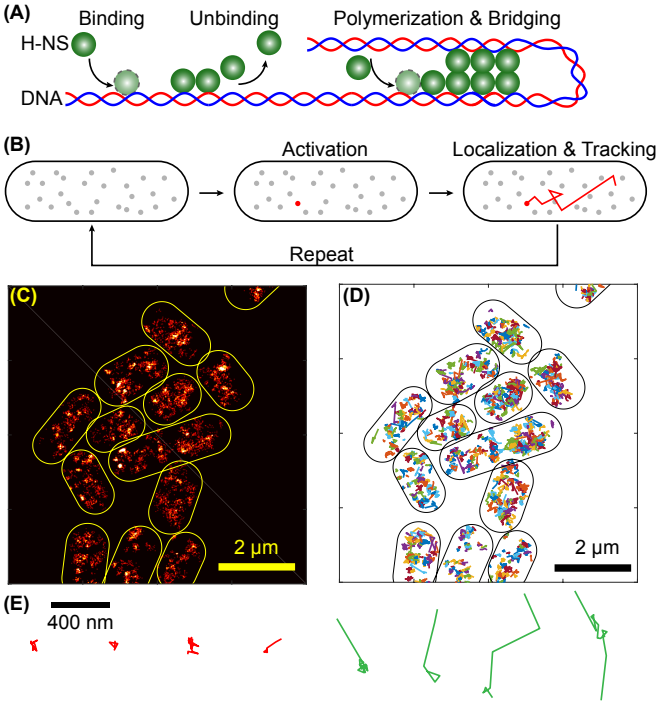

FIG. 1. (A) Illustration of H-NS proteins' key activities. H-NS is a DNA-binding protein, consisting of a DNA-binding domain, a linker, and an oligomerization domain, which allows H-NS to form polymers and DNA brdiging. (B) SptPALM for tracking H-NS proteins in live *E. coli*. (C) An example of super-resolved images of H-NS proteins in individual *E. coli*. (D) Examples of trajectories of H-NS proteins in the same area of (C). (E) Examples of individual trajectories.

From the trajectories, the mean-square-displacements (MSD) were calculated $\langle \Delta r^2(\tau) \rangle = \langle (\mathbf{r}(t+\tau) - \mathbf{r}(t))^2 \rangle$. The ensemble-averaged MSD from 38,796 trajectories with a minimum length of 10 frames (from 933 bacteria) was shown in Fig. 2A, where the error bars (smaller than the symbols) represented the standard error of the mean (SEM). The ensemble-averaged MSD bent down, clearly deviating from a straight line and indicating the sub-diffusive motion of H-NS proteins. Such anomalous diffusion of proteins and DNA inside bacteria [4, 12, 13], as well as proteins and lipids on the membranes of bacteria and cells (reviewed in [26]), have been observed previously. Fitting the MSD with $\langle \Delta r^2 \rangle = 4D\tau^\alpha$ gave the generalized apparent diffusion coefficient $D = (8.0 \pm 0.3) \times 10^3$ nm^2/s$^\alpha$ and the anomalous scaling exponent $\alpha = 0.57 \pm 0.02$. It is noted that the unit of the generalized apparent diffusion coefficient D contains the anomalous scaling exponent α. Alternatively, one can fit the MSD in short-time scale with a

simple line, $\langle \Delta r^2 \rangle = 4D_s\tau$, where D_s has the same unit of standard diffusion coefficients (m^2/s). Fitting the first three data points in the MSD curve in Fig. 2A gave $D_s = (24 \pm 7) \times 10^3$ nm^2/s, three times larger than the *numerical value* of the generalized diffusion coefficient. This is expected for sub-diffusive motion as the MSD curve bends *down*. The apparent short-time diffusion coefficient of H-NS proteins ($D_s \approx 0.024$ $\mu m^2/s$), is much lower than that of RNA polymerases (0.24 $\mu m^2/s$ [12] or RelA proteins ($0.03 - 3$ $\mu m^2/s$ [14]) in live *E. coli*, but similar to that of ribosomes (0.04 $\mu m^2/s$ [13]). Interestingly, the value of the generalized diffusion coefficient $D \approx 0.008$ $\mu m^2/s^{0.6}$ is in the same order as the chromosomal DNA of *E. coli* ($\sim$0.002 $\mu m^2/s^{0.4}$ [4]). This is expected because most, if not all, H-NS proteins are likely to bind to, and move together with, the chromosomal DNA. The anomalous scaling exponent $\alpha \approx 0.6$ of the H-NS proteins is different from that for the monomers of the chromosomal DNA ($\sim$0.35) or the center of mass ($\sim$0.7) [4, 27]. These differences in both D and α suggest that the motion of H-NS proteins is, although highly related to, different from the motion of the chromosomal DNA in bacteria.

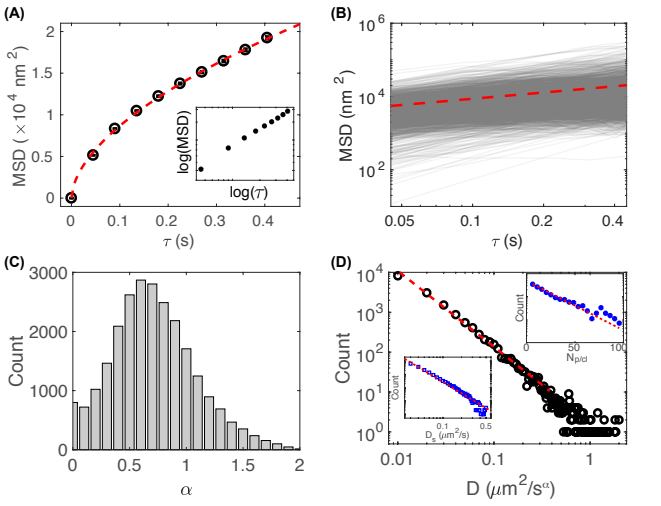

FIG. 2. (A) Ensemble-averaged MSD ($\circ$) from 38,796 trajectories (error bar: SEM). Fitting the data via $MSD = 4D\tau^\alpha$ gives $D = (8.0 \pm 0.3) \times 10^3$ nm^2/s and $\alpha = 0.57 \pm 0.02$ (red dashed line). Inset: log-log plot of the same data. (B) MSD of 2,000 individual trajectories (gray lines) in log-log scale, overlapped with the fitted ensemble-average (red dashed line). (C) Distribution of the anomalous exponent α. (D) Distribution of the generalized apparent diffusion coefficients fitted with $P(D) \propto D^{-(\beta+1)}$ (red dashed line, $\beta = 0.97 \pm 0.07$). Left-bottom inset: distribution of the short-time apparent diffusion coefficients, $P(D_s)$. Right-top inset: distribution of the number of proteins per cluster fitted with $P(n) \propto p^n$ (red dashed line, $p = 0.952 \pm 0.004$).

The heterogeneity in the dynamic diffusion of H-NS proteins was further investigated: in addition to the ensemble-averaged MSD, we examined the time-averaged MSD for each trajectory. Examples of MSD curves from 2000 trajectories are shown in log-log scale in Fig. 2B (gray lines), where the ensemble-averaged MSD is also shown (red dashed line). Each MSD curve was fitted, giving the fitted α and D values, whose distributions are shown in Fig. 2C and 2D. To minimize the effect of statistical and fitting errors, only the first half of the MSD was used for fitting, and only the ones with a good fitting ($R^2 > 0.95$) were selected for analysis. It was observed that the distribution of α is broad and peaked at 0.6, indicating that the most probable value is close to the ensemble average. However, the mean ($\sim$ 0.71, with a standard deviation of 0.37) is slightly higher than the ensemble average, possibly indicating weak non-ergodicity, a phenomenon reported previously for live systems [3]. In addition, we note that the distribution of α shows a population with $\alpha > 1$ (Fig. 2C). We speculate that this population is due to several possible reasons: 1) uncertainties in our experimental measurements, i.e., the finite precision in localizing the H-NS molecules, 2) fitting errors when obtaining D and α from individual MSD curves, and 3) possible active bacterial processes that result in actual super-diffusive motions. The existence of active motion of H-NS proteins was verified in two ways. First, we checked the individual MSD curves that gave $\alpha > 1$, and found that some of these curves are long and clean (Fig. S1A), in which fitting errors are likely very small. Second, we treated the bacteria in the exponential growth phase by 3.7% formaldehyde (HCHO) and produced (partially) dead and fixed bacteria. As expected, the HCHO treated bacteria displayed slower ensemble-averaged diffusion and lower anomalous scaling exponent (Fig. S1B). In addition, compared to the untreated ones, the distribution of α clearly shifted to the left (Fig. S1C) for the HCHO treated bacteria. We also quantified that the fraction of the $\alpha > 1$ population ($\psi_{\alpha>1}$) decreased from 20% to 12% (Fig. S1C) after HCHO-treatment.

More interestingly, the distribution of the *numerical values* of the generalized diffusion coefficients D is not peak-shaped; instead, it follows a power law, $P(D) \sim D^{-(\beta+1)}$, while fitting the data yields $\beta = 0.94 \pm 0.07$. The observed power-law for D is different from the behavior of Kaede proteins, RNA polymerases and ribosomes [12, 13, 28, 29]. For example, the RNA polymerase (another DNA binding protein) showed two peaks in the distribution of D, corresponding to the bound and unbound populations [12]. A note to make is that direct comparison and statistics on the generalized diffusion coefficient D is not stringent because 1) the unit of D contains the anomalous exponent α, and 2) the fitted α is different for different individual MSD curves. To address this concern, we calculated the short-time apparent diffusion coefficient D_s, which has a unit of nm^2/s and thus is good for direct comparison and statistics. We verified that D_s also showed a power-law distribution (Fig. 2D, left-bottom inset), indicating that the power-law distribution of H-NS proteins' diffusion coefficients is robust.

We speculated that the power-law distribution of D for H-NS proteins originates from their polymerization. As-

suming the polymerization of H-NS proteins is a process of adding monomers (i.e., the step-growth polymerization), then the probability of having a polymer of H-NS with a size of n is $P(n) \propto p^n$ where p is proportional to the concentration of monomers [30–33]. Evidence supporting this assumption came from experimentally examining the clustering of H-NS proteins. Briefly, the bacteria were fixed and imaged using super-resolution fluorescence microscope [19], followed by clustering analysis [34] and counting the number of H-NS proteins per cluster $N_{p/cl}$. Data from this simple analysis supported that $N_{p/cl}$ follows the assumed distribution, $P(n) \propto p^n$ (right-top inset of Fig. 2D, $p = 0.952 \pm 0.004$). However, we point out that further experiments are required to verify our assumption of the polymerization kinetics of H-NS proteins. It is expected that the polymerization of H-NS proteins slows down their diffusion; for example, ideal-chain polymers in ideal simple solutions show $D \sim n^{-1/2}$ because the diffusion coefficient is proportional to the inverse of the hydrodynamic size a (Stokes-Einstein equation), which is in turn proportional to $\sqrt{n}$ [35]. In general, we expect that $D(n) = D_1 n^{-1/\beta}$ where D_1 and β are two constants. Following this path, the cumulative probability for the diffusion coefficient can be obtained by

$$F(D(n) \leq D) = F(D_1 n^{-1/\beta} \leq D) \quad (1)$$

$$= 1 - F\left(n \leq (D_1/D)^{\beta}\right) \quad (2)$$

With $F(n)$ obtained from $P(n)$ with proper normalization, we have $F(n \leq N) = 1 - p^N$, and thus, $F(D(n) \leq D) = p^{(D_1/D)^{\beta}}$. As p was measured to be around 1, we can expand $F(D(n) \leq D)$ around $q = 1 - p \approx 0$ and ignore higher order terms,

$$F(D(n) \leq D) \approx 1 - (1-p) \cdot (D_1/D)^{\beta} \quad (3)$$

Therefore, the expected probability for D would be

$$P(D) = F'(D) \approx (1-p)\beta D_1^{\beta} \cdot D^{-(\beta+1)} \propto D^{-(\beta+1)} \quad (4)$$

, which predicts the experimental results (Fig. 2D). The measured exponent β deviated from 2, indicating that the H-NS polymers behave far from ideal chains and/or the environment of H-NS polymers is not an ideal simple fluid.

B. Unexpected distribution of displacement in H-NS proteins' diffusion

The dynamic diffusion of H-NS proteins is non-Brownian and anomalous (Fig. 2); more interestingly, it is non-Gaussian, non-Laplacian, and non-Cauchy. We calculated the displacements from the trajectories, $\Delta x = x(t_{i+1}) - x(t_i)$ and $\Delta y = y(t_{i+1}) - y(t_i)$, and the corresponding distributions, $P(\Delta x)$ and $P(\Delta y)$ are shown in Fig. 3A and 3B (black circles), respectively. Compared to the Gaussian distribution (red dot dashed lines), the measured distributions show heavy tails at larger displacements. In addition, our data from H-NS proteins cannot be fitted with the Laplace distribution (brown dotted lines), which has been successfully applied to the motion of protein-bound RNA molecules in live *E. coli* and yeast [5]. We note that the heavy tails are unlikely caused by measurement errors: when restricting the calculations on trajectories showing $0.3 \leq \alpha \leq 0.7$, the same distributions were observed and the heavy tails were present. The heavy tails are reminiscent of the (Mandelbrot) Levy flights, which shows a Cauchy distribution for displacments [36]. However, the displacement distributions for H-NS proteins do not follow the Cauchy distribution (magenta dashed line). Instead, the distribution of H-NS displacement can be fitted well with the Pearson Type VII distribution (green solid line), $P(\Delta x) \propto \left(1 + \Delta x^2/w^2\right)^{-m}$, which is a rarely used generalization of the Gaussian distribution and Cauchy distribution [37]. To confirm that the Pearson Type VII distribution is indeed the best fit to the data among the four aforementioned distributions, we calculated the fitting errors using $\delta = \sum_i \frac{|\log(f_i) - \log(m_i)|}{\log(m_i)}$ and $\chi^2 = \sum_i \frac{(\log(f_i) - \log(m_i))^2}{\log(m_i)}$, where f_i are the fitted values and m_i the measurements. It is noted that, to be consistent with the logarithm scale of the y-axis in Fig. 3A and 3B, $\log(f_i)$ and $\log(m_i)$ were used for estimating the fitting errors. It was confirmed that the Pearson Type VII distribution yielded the lowest δ and χ^2 for both Δx and Δy, as shown in Fig. 3C.

It was suggested that the velocity/displacement distribution of motor proteins follow the Pearson Type VII distribution in the presence of detachment events [38], indicating that the observed displacement distributions of H-NS proteins might be related to the dynamic binding/unbinding of H-NS proteins on DNA. To pursue this concept, we modeled that the molecules display a slower motion in the DNA-bound state (B) and a faster motion in the unbound state (U) as shown in the inset of Fig. 3D and ran Monte Carlo simulations. The diffusion coefficients of the H-NS molecules used in the simulations were $D_u = 2.4 \times 10^5$ nm^2/s and $D_b = 2.4 \times 10^4$ nm^2/s for the unbound and bound states, respectively. In each state, the displacements of the molecules were from the Brownian motion, i.e., $\Delta x = \sqrt{2\ D\ dt} \cdot \xi$ where $D = D_u$ or D_b, $dt = 45$ ms, and ξ is a random variable following the standard normal distribution. In addition, the molecules switch states dynamically, with probabilities of p_{bu} (from the bound state to the unbound state) and p_{ub} (from the unbound state to the bound state), respectively. As the events with large displacements are rare in Fig. 3A and 3B, it is expected that p_{ub} is high but p_{bu} is low. Therefore, we used $p_{ub} = 0.96$ and $p_{bu} = 0.02$ for the Monte Carlo simulations. We repeated 100 simulations, and each simulation consisted of 1000 trajectories with lengths of randomly 4 – 100 steps. From all the simulations, the distribution of the displacement Δx was calculated. As shown in Fig. 3D, the simulated results (blue triangles) overlap well with the experimental

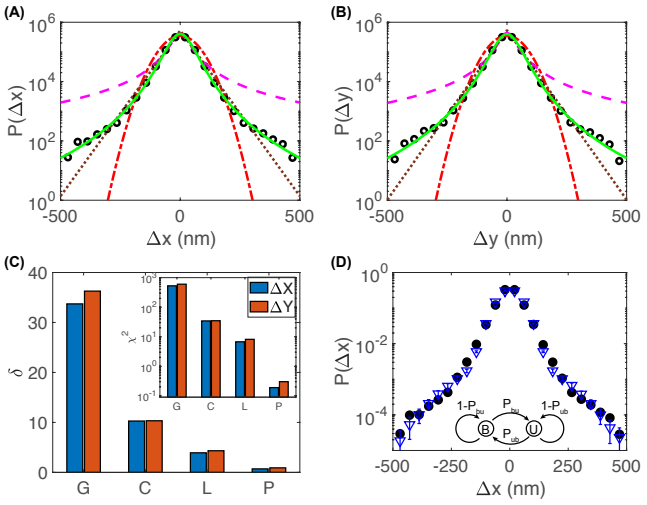

FIG. 3. (A, B) Distribution of displacements (A: Δx, B: Δy). The experimental data (black circles) cannot be fitted with the Gaussian (red dot-dashed line), Cauchy (magenta dashed line), or Laplace (brown dotted line) distributions. Instead, the Pearson Type VII distribution (green solid line) fits the data very well. (C) Fitting errors δ from the fittings of the data using the Gaussian (G), Cauchy (C), Laplace (L) and Pearson Type VII (P) distributions. Inset: χ^2 of the fittings. (D) Distribution of displacement from Monte Carlo simulations (blue triangles) overlapping with the experimental measurements (black circles, same data as in [A]). Inset: the Monte Carlo simulations assume that the molecules can switch between a bound state (B, slow diffusion) and an unbound state (U, fast diffusion) with rates of p_{ub} (U to B) and p_{bu} (B to U).

data (black circles). It is noted that the purpose of the current model/simulation is to explore the possibility to attribute the observed displacement distribution to the binding/unbinding of H-NS proteins on DNA. However, the current model is far from a complete description of the dynamics of H-NS proteins in live bacteria; for example, both the anomalous diffusion and polymerization of H-NS proteins have been omitted in the current model. More sophisticated models and simulations will be presented in future works.

C. Viscoelasticity of bacterial cytoplasm

It has been reported previously that the bacterial cytoplasm is viscoelastic [1, 4]. For example, Weber et al. examined the velocity auto-correlation of chromosomal loci in *E. coli* based on fractional Langevin equation, and showed that the cytoplasmic viscoelasticity causes negative velocity auto-correlations at short times [4, 27]. We observed similar results from the dynamics of H-NS proteins: the velocity auto-correlation can be fitted very well by Weber's formula [4, 27] (Fig. 4A), clearly confirming the viscoelasticity of the bacterial cytoplasm. As the distinction between fractional Brownian motion and continuous-time random walk (CTRW) in cellular dynamics has recently caught interests of many physicists, it is worthwhile to mention that our observations are less consistent with the CTRW process for the following two reasons. First, the negative velocity auto-correlation supports the fractional Brownian motion as opposed to CTRW [4, 5, 27]. Second, if it were a CTRW process, a second, shallower slope is expected in the MSD curve, which is however missing in our experimental measurements (Fig. 2A).

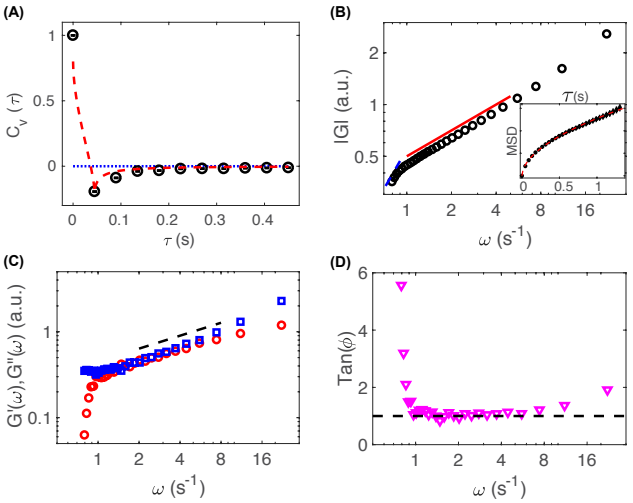

FIG. 4. (A) Velocity autocorrelation of H-NS proteins is negative at short time-scales. (B) Frequency dependence of the magnitude of the complex modulus $|G(\omega)|$ of bacterial cytoplasm. Inset: the ensemble-averaged MSD curve with longer τ. (C) Frequency dependence of the storage (red circles) and loss (blue squares) modulii, $G'(\omega)$ and $G''(\omega)$. (D) Frequency dependence of $\tan\phi = G''/G'$.

We further examined the viscoelasticity of the cytoplasm that H-NS proteins experienced by looking at the complex modulus $G(\omega)$, which is related to the memory kernel $K(t) = (2-\alpha)(1-\alpha)/|t|^\alpha$ in the fractional Langevin equation [4, 39],

$$G(\omega) \propto i\omega \int_{-\infty}^{+\infty} K(t) e^{-i\omega t} dt \propto \omega^\alpha \cdot e^{-i\alpha\pi/2} \qquad (5)$$

Therefore, under this assumption, the magnitude ($|G(\omega)|$), the storage modulus ($G'(\omega) = \Re\{G(\omega)\}$) and the loss modulus ($G''(\omega) = \Im\{G(\omega)\}$) are all expected to be proportional to ω^α. This single-exponent power-law behavior has been observed experimentally for homogeneous protein solutions [40], indicating that the fractional Langevin equation can account for the viscoelasticity of homogeneous protein solutions. However, we found that the viscoelasticity of bacterial cytoplasm is more complicated than this single-exponent power law. To see this, we calculated the magnitude of the complex modulus,

the storage and loss modulii, following Ref. [40–42],

$$|G| = \frac{k_B T}{\pi a} \cdot \frac{1}{\langle \Delta r^2(1/\omega)\rangle \Gamma(1+\alpha(\omega))} \quad (6)$$

$$G' = |G|\cos(\pi\alpha(\omega)/2) \quad (7)$$

$$G'' = |G|\sin(\pi\alpha(\omega)/2) \quad (8)$$

where

$$\omega = 1/\tau \quad (9)$$

$$\alpha(\omega) = \left.\frac{d\ln\langle\Delta r^2(\tau)\rangle}{d\ln\tau}\right|_{\tau=1/\omega} \quad (10)$$

As shown in Fig. 4B, the magnitude $|G(\omega)|$ displays at least two different slopes in the log-log scale. For $\omega > 1$ s^{-1}, the power-law exponent is ~ 0.5 (red solid line), while for low frequencies $\omega < 1$ s^{-1}, the slope becomes ~ 1.5 (blue dashed line). This transition is more obvious in the plots for the real and imaginary parts ($G'(\omega)$ and $G''(\omega)$, Fig. 4C). The loss modulus ($G''(\omega)$) remained constant below $\omega = 1$ s^{-1} while the storage modulus ($G'(\omega)$) decreased quickly. In addition, we note that the slopes start to become different at high frequencies ($\omega \gtrsim 10$ s^{-1}). Furthermore, we looked at the transition by plotting the ratio between the loss modulus and the storage modulus, $\tan\phi = G''/G'$, which has been used for categorize materials ($\gg 1$ for viscous liquids, $\ll 1$ for elastic solids, and ~ 1 for viscoelastic materials) [43]. As shown in Fig. 4D, at low frequencies (long time scales), the cytoplasm of *E. coli* behaves more like viscous liquids, while at high-enough frequencies (short-enough time scales), the cytoplasm becomes viscoelastic, suggesting a possible glass-liquid transition in the frequency domain and supporting the work by Parry et al. [1]. In addition, the time/frequency dependence of the complex modulus suggests the so-called aging effect: the dynamics changes over time [2, 44].

D. Age-dependence of H-NS proteins' diffusion

Furthermore, we attempted to probe whether the dynamics of H-NS proteins is dependent on cell-age. For *E. coli*, the cell-age can be easily read from the cell-length, as the cell-age is nearly linear to the cell-length [45]. As the lengths of individual bacteria ranged from 1 μm to 6 μm, we picked cells from three groups: < 1.2 μm, $2.8-3.0$ μm, and > 5 μm, followed by calculating the MSD for the trajectories in the cells in each group. As shown in Fig. 5A, the MSD moved up as the cell lengths increased (< 1.2 μm: red circles, $2.8-3.0$ μm: magenta squares, > 5 μm: blue triangles). The age-dependence of H-NS proteins' dynamics can also be seen from the radius of gyration R_g of the trajectories [1, 46], which shifted to higher values (Fig. 5B). In addition, by fitting the MSD curves, we found that cell aging caused D to increase (Fig. 5C), while α did not change significantly (Fig. 5D). We note that, to our knowledge, the observed cell-to-cell variability in the H-NS proteins diffusional dynamics was not reported previously.

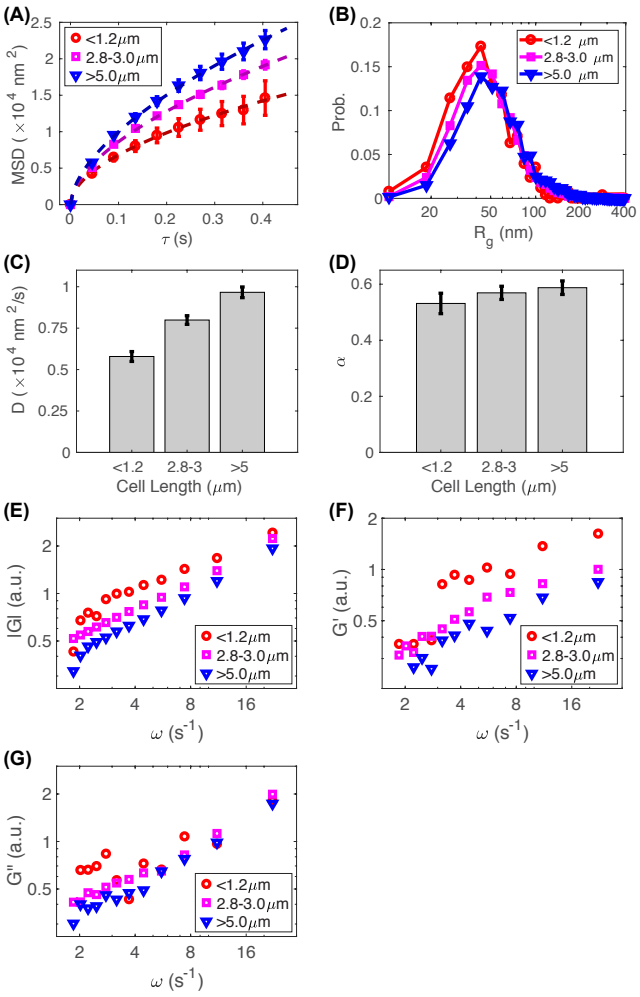

FIG. 5. (A) Ensemble-averaged MSD for bacteria with different lengths (< 1.2 μm: red circles, $2.8-3.0$ μm: magenta squares, > 5 μm: blue triangles). Error bars = SEM. (B) Radius of gyration R_g of trajectories for the cells from the three groups. (C) Fitted diffusion coefficients from (A). (D) Fitted exponents α from (A). Error bars in (C) and (D) represent fitting errors. (E) Comparison of the magnitude of the complex modulus $|G(\omega)|$ of bacterial cytoplasm between bacteria with different lengths. (F) Comparison of the storage modulus $G'(\omega)$ of bacterial cytoplasm between bacteria with different lengths. (G) Comparison of the loss modulus $G''(\omega)$ of bacterial cytoplasm between bacteria with different lengths.

The observed age-dependence is unlikely size-effect because the cell-length is always greater than the cell-diameter of *E. coli* and the latter is expected to be the limiting factor. An alternative hypothesis is that the age-dependence of H-NS proteins' diffusional dynamics might reflect the changes in the bacterial metabolism when they grow. This is because metabolism fluidized the bacterial cytoplasm [1], and, according to the Kleiber's law, a larger body size gives higher metabolic rate [47]. To

test this hypothesis, the viscoelasticity of the bacterial cytoplasm for the cells in the three length/age groups was examined by calculating the complex moduli ($|G(\omega)|$, $G'(\omega)$ and $G''(\omega)$, Fig. 5E–G) for the three groups (< 1.2 μm, $2.8 - 3.0$ μm, and > 5 μm) from the MSD curves (Fig. 5A) as described above. We observed that the magnitude of the complex moduli ($|G(\omega)|$) decreases as the cell length/age increases (Fig. 5E), suggesting that movement of proteins in longer cells is indeed easier (i.e., given the same stress σ, the resultant strain ϵ is higher for smaller complex modulus, $|\epsilon| = |\sigma|/|G|$). Therefore, this observation supports the hypothesis that the cytoplasm of longer bacteria is more fluidized than shorter ones. More interestingly, we found that the underlying reason for the cytoplasmic fluidization as the cells grow depends on the time-scale (i.e., the frequency ω). For example, differences in the storage moduli (elasticity) at higher frequencies ($\omega \geq 3$ s^{-1}) are more prominent than at the lower-frequency range (Fig. 5F). In contrast, the loss moduli (viscosity) showed the opposite: larger changes were observed at lower frequencies (Fig. 5G).

IV. CONCLUSIONS

To conclude, we investigated the dynamics of H-NS proteins in live *E. coli* bacteria using super-resolution fluorescence microscopy in combination with single-particle tracking. Apart from the sub-diffusive behavior, a new power-law distribution was observed for the diffusion coefficients of individual H-NS proteins, which can be attributed to the polymerization of the proteins. It is observed that the distribution of displacements of H-NS proteins was non-Gaussian or non-Cauchy. In addition, rather than the Laplace distribution, which was applied successfully to other molecules in *E. coli* and yeast, the Pearson Type VII distribution is needed to fit the data for H-NS proteins. Furthermore, the dynamics of H-NS proteins reports the viscoelasticity of the bacterial cytoplasm; more importantly, we experimentally measured, for the first time, the frequency dependence of the complex modulus of the cytoplasm of live bacteria, which is much more challenging than those for eukaryotic cells [42, 48] due to the much smaller size of bacteria. In addition, we found that the viscoelasticity of bacterial cytoplasm shows a glass-liquid transition, different from homogeneous protein solutions. The measured transition also differs quantitatively from those observed for eukaryotic cytoplasms [42, 49]. Lastly, we examined the dependence of the dynamics of H-NS proteins on cell-length (and thus cell-age), and found that the dynamics of H-NS proteins slows down as the bacteria become longer. To our knowledge, this is the first observation of size-dependence and cell-to-cell variability in diffusion characteristics of proteins in live bacteria.

Our findings are expected to fundamentally change the way how the bacterial cytoplasm is viewed: unlike a simple viscous or viscoelastic fluid that current models of bacterial processes typically consider, the bacterial cytoplasm behaves differently at different time scales in terms of mechanical properties, which is expected to impact various interactions among small molecules, proteins and DNA/RNA molecules inside bacteria, as well as bacterial interactions with other species, such as bacteriophages.

V. ACKNOWLEDGMENT

This work was supported by the University of Arkansas and the Arkansas Biosciences Institute (ABI-0189, ABI-0226, ABI-0277). We thank Giovanni Zocchi for carefully reading the manuscript and giving insightful comments.

[1] B. R. Parry, I. V. Surovtsev, M. T. Cabeen, C. S. O'Hern, E. R. Dufresne, and C. Jacobs-Wagner, Cell **156**, 183 (2014).
[2] R. Metzler, Biophysical Journal **112**, 413 (2017).
[3] J.-H. Jeon, V. Tejedor, S. Burov, E. Barkai, C. Selhuber-Unkel, K. Berg-Sørensen, L. Oddershede, and R. Metzler, Phys. Rev. Lett. **106**, 048103 (2011).
[4] S. C. Weber, A. J. Spakowitz, and J. A. Theriot, Phys. Rev. Lett. **104**, 238102 (2010).
[5] T. J. Lampo, S. Stylianidou, M. P. Backlund, P. A. Wiggins, and A. J. Spakowitz, Biophysical Journal **112**, 532 (2017).
[6] E. Betzig, G. H. Patterson, R. Sougrat, O. W. Lindwasser, S. Olenych, J. S. Bonifacino, M. W. Davidson, J. Lippincott-Schwartz, and H. F. Hess, Science (New York, N.Y.) **313**, 1642 (2006).
[7] M. Bates, B. Huang, G. T. Dempsey, and X. Zhuang, Science (New York, N.Y.) **317**, 1749 (2007).
[8] B. Huang, W. Wang, M. Bates, and X. Zhuang, Science (New York, N.Y.) **319**, 810 (2008).
[9] M. Heilemann, S. Van De Linde, A. Mukherjee, and M. Sauer, Angewandte Chemie - International Edition **48**, 6903 (2009).
[10] Y. Wang, G. Fruhwirth, E. Cai, T. Ng, and P. R. Selvin, Nano Letters **13**, 5233 (2013).
[11] S. Manley, J. M. Gillette, G. H. Patterson, H. Shroff, H. F. Hess, E. Betzig, and J. Lippincott-Schwartz, Nat Meth **5**, 155 (2008).
[12] M. Stracy, C. Lesterlin, F. Garza de Leon, S. Uphoff, P. Zawadzki, and A. N. Kapanidis, Proceedings of the National Academy of Sciences **112**, E4390 (2015).
[13] S. Bakshi, A. Siryaporn, M. Goulian, and J. C. Weisshaar, Molecular Microbiology **85**, 21 (2012).
[14] W. Li, E. Bouveret, Y. Zhang, K. Liu, J. D. Wang, and J. C. Weisshaar, Molecular Microbiology **99**, 571 (2016).
[15] K. J. Barns and J. C. Weisshaar, Biochimica et Biophysica Acta (BBA) - Biomembranes **1858**, 725 (2016).
[16] J. Salje, P. Gayathri, and J. Löwe, Nature reviews. Microbiology **8**, 683 (2010).

[17] C. J. Dorman, Nature Reviews Microbiology **2**, 391 (2004).
[18] Y. Gao, Y. H. Foo, R. S. Winardhi, Q. Tang, J. Yan, and L. J. Kenney, PNAS **114**, 12560 (2017).
[19] A. Mazouchi and J. N. Milstein, Bioinformatics **32**, 747 (2016).
[20] M. Zhang, H. Chang, Y. Zhang, J. Yu, L. Wu, W. Ji, J. Chen, B. Liu, J. Lu, Y. Liu, J. Zhang, P. Xu, and T. Xu, Nature methods **9**, 727 (2012).
[21] Y. Wang, P. Penkul, and J. N. N. Milstein, Biophysical Journal **111**, 467 (2016).
[22] A. Edelstein, N. Amodaj, K. Hoover, R. Vale, and N. Stuurman, in *Current Protocols in Molecular Biology* (John Wiley & Sons, Inc., Hoboken, NJ, USA, 2010).
[23] S. Wolter, A. Löschberger, T. Holm, S. Aufmkolk, M.-C. Dabauvalle, S. V. D. Linde, M. Sauer, and S. van de Linde, Nature methods **9**, 1040 (2012).
[24] J. C. Crocker and D. G. Grier, Journal of Colloid and Interface Science **179**, 298 (1996).
[25] S. Wang, J. R. Moffitt, G. T. Dempsey, X. S. Xie, and X. Zhuang, Proceedings of the National Academy of Sciences of the United States of America **111**, 8452 (2014).
[26] R. Metzler, J. H. Jeon, and A. G. Cherstvy, Biochimica et Biophysica Acta (BBA) - Biomembranes Biosimulations of lipid membranes coupled to experiments, **1858**, 2451 (2016).
[27] S. C. Weber, J. A. Theriot, and A. J. Spakowitz, Phys. Rev. E **82**, 011913 (2010).
[28] S. Bakshi, B. P. Bratton, and J. C. Weisshaar, Biophysical Journal **101**, 2535 (2011).
[29] N. A. Licata, B. Mohari, C. Fuqua, and S. Setayeshgar, Biophysical Journal **110**, 247 (2016).
[30] R. Phillips, J. Kondev, and J. Theriot, *Physical Biology of the Cell* (Garland Science, 2013).
[31] W. H. Stockmayer, Journal of Polymer Science **9**, 69 (1952).
[32] P. J. Flory, J. Am. Chem. Soc. **58**, 1877 (1936).
[33] S. Kéki, M. Zsuga, and A. Kuki, J. Phys. Chem. B **117**, 4151 (2013).
[34] F. Levet, E. Hosy, A. Kechkar, C. Butler, A. Beghin, D. Choquet, and J.-B. Sibarita, Nature Methods **12** (2015), 10.1038/nmeth.3579.
[35] M. Rubinstein and R. H. Colby, *Polymer Physics*, 1st ed. (Oxford University Press, Oxford ; New York, 2003).
[36] M. L. Ackerman, P. Kumar, M. Neek-Amal, P. M. Thibado, F. M. Peeters, and S. Singh, Phys. Rev. Lett. **117**, 126801 (2016).
[37] K. Pearson, Phil. Trans. R. Soc. Lond. A **216**, 429 (1916).
[38] J. Hughes, S. Shastry, W. O. Hancock, and J. Fricks, JABES **18**, 204 (2013).
[39] Y. Wang and G. Zocchi, PLoS ONE **6**, e28097 (2011).
[40] W. Pan, L. Filobelo, N. D. Q. Pham, O. Galkin, V. V. Uzunova, and P. G. Vekilov, Phys. Rev. Lett. **102**, 058101 (2009).
[41] T. G. Mason, Rheol. Acta **39**, 371 (2000).
[42] D. Wirtz, Annu. Rev. Biophys. **38**, 301 (2009).
[43] J. D. Ferry, *Viscoelastic Properties of Polymers, 3rd Edition*, 3rd ed. (Wiley, New York, 1980).
[44] R. Metzler, J.-H. Jeon, A. G. Cherstvy, and E. Barkai, Phys. Chem. Chem. Phys. **16**, 24128 (2014).
[45] L. Robert, M. Hoffmann, N. Krell, S. Aymerich, J. Robert, and M. Doumic, BMC Biology **12**, 17 (2014).
[46] Y. S. Hu, H. Cang, and B. F. Lillemeier, Proceedings of the National Academy of Sciences **113**, 7201 (2016).
[47] M. Kleiber, Physiological Reviews **27**, 511 (1947).
[48] Y. Tseng, T. P. Kole, and D. Wirtz, Biophysical Journal **83**, 3162 (2002).
[49] B. D. Hoffman, G. Massiera, K. M. V. Citters, and J. C. Crocker, PNAS **103**, 10259 (2006).

SUPPLEMENTARY INFORMATION

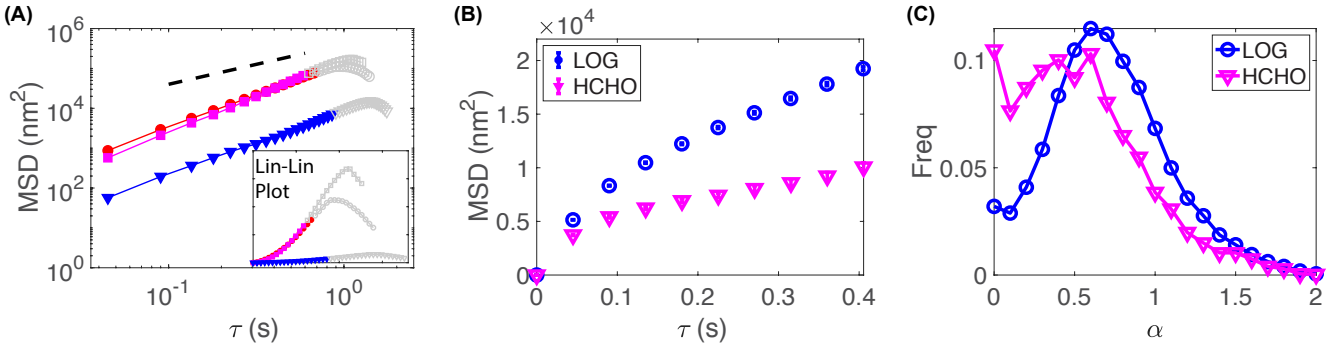

FIG. S1. (A) Examples of long MSD curves (> 20 frames) showing super-diffusive motions (i.e., steeper than the slope of one, which is shown as a black dashed line). The colored portions of the curves were used for fittings to obtain the generalized diffusion coefficient and the anomalous scaling exponent, $MSD = 4D\tau^{\alpha}$. Inset: the MSD curve plotted in linear scales. (B) Ensemble averaged MSD curves for bacteria in the exponential growth phase (or log phase, LOG) and bacteria treated with formaldehyde (HCHO). (C) Distribution of the anomalous scaling exponent α for untreated bacteria in the exponential growth phase (LOG) and treated bacteria with formaldehyde (HCHO).